Bifurcation to oscillatory flow of the natural convection around a vertical channel in rectangular enclosure

J.P. Liu and W.Q. Tao
School of Energy and Power Engineering, Xi'an Jiaotong University, Shaanxi, PR China

Keywords *Bifurcation, Channels, Enclosures, Natural convection, Numerical analysis*

Abstract *Numerical computations were performed for the heat transfer and fluid flow characteristics of natural convection with an internal vertical channel composed by a pair of parallel plates in a rectangular enclosure. The inner plates and the bounding wall of the enclosure were maintained at uniform but different temperatures. The plates were symmetrically arranged. Unsteady computation was performed to simulate the evolution process of the natural convection developing from the zero initial field. The cases of* $Ra = 2 \times 10^4$, 2×10^5 *and* 10^6 *were studied. A symmetrical steady solution was achieved for the case of* $Ra = 2 \times 10^4$. *For* $Ra = 2 \times 10^5$ *and* 10^6, *time dependent asymmetrical processes were observed. The flow oscillating process seemed to be more complex at* $Ra = 2 \times 10^5$ *than that at* $Ra = 10^6$, *which is quasi-periodic with two frequencies.*

Nomenclature

- a = thermal diffusivity
- A_c = component of the amplitude defined by equation 9
- A_m = amplitude by equation 10
- A_s = component of the amplitude defined by equation 8
- b = half width of the enclosure
- B = dimensionless half width of the enclosure
- h = height of the channel plate
- k_f = fluid thermal conductivity
- k_s = solid thermal conductivity
- K = relative thermal conductivity
- l = distance from the top of the plate to the top wall of the enclosure, i.e., distance from the bottom of the plate to the bottom wall of the enclosure
- L = dimensionless value of l
- M_{res} = mass residual
- Nu = average Nusselt number
- Nu_{IL} = average Nusselt number inside the left plate
- Nu_{IR} = average Nusselt number inside the right plate
- Nu_{OL} = average Nusselt number outside the left plate
- Nu_{OR} = average Nusselt number outside the left plate
- p' = effective pressure
- P = dimensionless pressure, defined as $P = p'/[(\rho(RaPr)/(a/h)^2]$
- Pr = Prandtl number
- Ra = Rayleigh number based on the height of the plate, h
- s = channel width
- S = dimensionless channel width, s/h
- t = time
- T = temperature
- T_1 = dimensionless temperature at the inlet of the channel on the middle vertical line
- T_2 = dimensionless temperature at the middle point in the channel
- T_3 = dimensionless temperature at the outlet of the channel on the middle vertical line
- T_h = temperature of the internal plate
- T_c = temperature of the enclosure surface
- u,v = velocity component in x-, y- direction
- U,V = dimensionless velocities, $U = u/u_r$, $V = v/u_r$
- u_r = reference velocity, defined as $(RaPr)^{1/2}/(a/h)$
- x,y = coordinates
- X,Y = dimensionless coordinates, $X = x/h$, $Y = y/h$

International Journal of Numerical Methods for Heat & Fluid Flow, Vol. 9 No. 2, 1999, pp. 170-185,

This work was supported by the Natural National Science Foundation of China.

Greek symbols

α_i = heat transfer coefficient
β = volume expansion coefficient
Δ = thickness of the plates
ν = kinetic viscosity
ρ = density of the fluid
Θ = dimensionless temperature, defined as $(T - T_c) / (T_h - T_c)$
τ = dimensionless time, defined as $u_r t/h$
τ_m = dimensionless period used in FFT

1. Introduction

Vertical channel formed by two parallel plates or fins is a frequently encountered configuration in thermal engineering, for example, the finned exchanger, the collector of solar energy, the core of nuclear reactors, and the cooling device of electronic and micro-electronic equipment. In many cases, the configuration is placed in a confined enclosure and the natural convection of the channel cannot be fully developed because of the limited space between the channel and the enclosure walls. The flow and heat transfer characteristics of such cases are obviously different from the case of a channel in infinite space. On the other hand, the basic feature of heat transfer and fluid flow of such cases are also different from those of natural convection in an enclosure without any internal isolated islands. In this paper, the numerical results of the bifurcation of natural convection in an enclosure with internal islands to oscillatory flow will be presented. To the authors' knowledge, the available literature contains no information about the Hopf bifurcation of natural convection in such kinds of configuration. Therefore, a review will be given to the two related problems, i.e., natural convection around a channel in a rectangular enclosure and Hopf bifurcation of natural convection in an enclosure without any internal bodies.

Adlam (1986) performed computations of transient two-dimensional natural convection in cavities with one or several internal isolated bodies. Among the configurations studied was the enclosure with two internal vertical thick plates placed symmetrically and heated to a constant temperature. The surrounding walls were cooled to a constant temperature. Only the case of Ra (based on the enclosure height) = 10^6 and Pr = 5.39 was computed. It was found that the flow in the enclosure was symmetrical and the stream function did not approach a constant value when time increased. Shyy and Rao (1993) conducted a transient numerical simulation for a similar configuration with zero plate thickness for which the Grashof number based on the chemical half width was 10^5 and Pr = 0.71. The cavity had adiabatic top and bottom walls with its two vertical surfaces maintained at constant temperature. Their results showed that when time approaches infinite, steady state solution does exist. In their computation, physical symmetry condition at the geometrically symmetric line at the enclosure was adopted and only half of the domain was taken into account. In the recent work performed by the Liu and Tao (1996) numerical results for the natural convection of air in the enclosure shown in Figure 1 were presented. The Rayleigh number based on the channel height h was varied from 10^2 to 10^7. Symmetric boundary condition at the enclosure center line was adopted. Transient and steady-state simulations were both conducted for the case of Ra = 10^6, and it was found that the numerical results of the transient solution agree with the steady-state solution quite well when time approaching infinite. The

computations revealed two flow patterns in the half domain: unicellular flow at low Rayleigh number and bicellular flow at higher Rayleigh number. It was found that the critical Rayleigh number for the transition of the unicellular flow to the bicellular flow was higher than the critical Rayleigh number related to the transition of the bicellular flow to the unicellular flow. Hence there is static flow bifurcation when the Rayleigh number is between the two critical Rayleigh numbers. However, the symmetry boundary condition at the geometrically symmetric line adopted in the papers of Shyy and Rao (1993) and Liu and Tao (1996) is open to discussion.

Bifurcation to oscillatory flow of natural convection of air in rectangular enclosure with no internal bodies has been numerically studied by a number of authors. Le Quere and Alziary de Roquefort (1985) studied the transition to unsteady natural convection of air in differentially heated vertical cavities with aspect ratio A = 4-10. Later (Le Quere and Alziary de Roquefort, 1986), they also calculated the stability for air in cavities of A = 1-10 with perfectly conducting walls. Winters (1987) developed a technique for locating Hopf bifurcations in steady-state equations to the problem of natural convection in a square, air-filled cavity with conducting boundaries. In 1988, Yang made a review on the experimental and numerical studies of flow instability, bifurcation, and transition to turbulence for natural convection in three-dimensional enclosures with emphasis on the Rayleigh-Benard problem (Yang, 1988). Henkes and Hoogendoorm (1990) made a comprehensive study on the stability of the natural convection in a square cavity heated from the side. From the works cited above, it can be certain that the aspect ratio of a 2-D cavity has a profound effect on the critical Rayleigh number beyond which the flow loses its stability. Besides, the natural convection turns to oscillatory flow at a lower Rayleigh number in the case of conducting horizontal walls than in the case of adiabatic horizontal walls. For example, the critical Rayleigh number for the air-filled enclosure with conducting horizontal walls is 2.24×10^5 and 2.2×10^6 for A = 10 and 1 respectively (Le Quere and Alziary de Roquefort, 1986). For the square

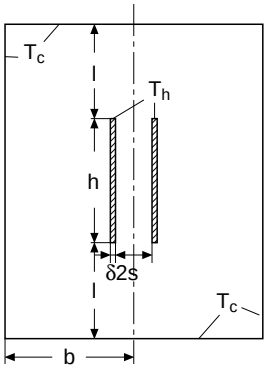

Figure 1.
Schematic diagram of configuration studied

enclosure with adiabatic horizontal walls, Henkes and Hoogendoorn obtained the critical Rayleigh number of 2×10^8 for air.

The purpose of the present study is twofold. First, by comparing the solutions for the entire geometry and for the half domain, the Rayleigh number range within which the two solutions are the same is examined. Second, by solving the transient, two-dimensional Navier-Stokes equations, the stability of the steady, two-dimensional laminar flow in the rectangular enclosure with internal islands is determined. The physical problem is depicted in Figure 1. The main parameters are as follows: h/l = 0.75, δ/l = 0.03, 2b/l=2, 2s/l = 0.4 and Pr = 0.7.

2. Mathematical formulation and numerical method

The following assumptions are adopted in the numerical analysis:

(1) the fluid in the enclosure is of Boussinesq type;

(2) the fluid flow and heat transfer is two-dimensional and laminar; and

(3) the dissipation term in the energy equation is neglected.

Using the definitions given in the nomenclature, we may obtain the following dimensionless governing equations:

$$\frac{\partial U}{\partial \tau} + U\frac{\partial U}{\partial X} + V\frac{\partial U}{\partial Y} + -\frac{\partial P}{\partial X} + \frac{\Pr}{\sqrt{Ra\,\Pr}}\left(\frac{\partial^2 U}{\partial X^2} + \frac{\partial^2 U}{\partial Y^2}\right) \tag{1}$$

$$\frac{\partial V}{\partial \tau} + U\frac{\partial V}{\partial X} + V\frac{\partial V}{\partial Y} = -\frac{\partial P}{\partial Y} + \frac{\Pr}{\sqrt{Ra\,\Pr}}\left(\frac{\partial^2 V}{\partial X^2} + \frac{\partial^2 V}{\partial Y^2}\right) + \Theta \tag{2}$$

$$\frac{\partial \Theta}{\partial \tau} + U\frac{\partial \Theta}{\partial X} + V\frac{\partial \Theta}{\partial Y} = \frac{K}{\sqrt{Ra\,\Pr}}\left(\frac{\partial^2 \Theta}{\partial X^2} + \frac{\partial^2 \Theta}{\partial Y^2}\right) \tag{3}$$

$$\frac{\partial U}{\partial X} + \frac{\partial V}{\partial Y} = 0 \tag{4}$$

The boundary conditions are as follows:

at the wall of the enclosure

$$U = V = \Theta = 0 \tag{5}$$

In addition, the following conditions must be satisfied for the internal solid plates:

$$U = V = 0, \Theta = 1 \tag{6}$$

The initial fields of our investigation were zero fields, i.e. the initial velocities and initial temperature were all zero except at the internal solid plates where initial dimensionless temperature was 1.

The governing equations were discretized by the finite volume approach. The central difference scheme (CDS) was adopted for the discretization of the convection-diffusion terms to decrease the numerical viscosity. The unsteady

terms in the equations were discretized by the full implicit scheme. The SIMPLEC algorithm was used. Special attention was paid to the treatment of the isolated solid region. In our work, the coefficients of the discretization equations were properly assigned to confirm the additional condition equation (6) in the solid region. Besides, the relative thermal conductivity $K(k_s/k_f)$ took the value of 1 in the fluid region and a very large value in the solid region. For details, refer to the literature of Yang and Tao (1992).

For the grid-point layout, we used the equally divided grid-points in the Y direction. In the X direction, non-equally divided grid system was used, which had the grid point concentrated near the solid plates, but sparse far from the plate. The grid system was selected as 120(X)X80(Y), this was the maximum value our personal computer could bear. Our preliminary computations show that the numerical solution of this grid system may be considered as grid-independent, and the grid systems used in other papers for investigating oscillatory convection were even coarser. The time step was chosen as $\tau = 0.25$. This value of time step was adopted after different time steps, 0.1, 0.25, 0.5 and 1, had been tried in our preliminary investigation for $Ra = 10^6$. This choice also may be evidenced by the following consideration. The dimensionless time periods of the oscillatory cycle found in the computation for the case of $Ra = 10^6$ were 23.5 and 46.7. This means that hundreds of time steps must be taken in order to simulate one oscillatory cycle.

In the computation for the entire domain, some special treatments were used to ensure the symmetry of the numerical treatment. The vertical center line was chosen as the interface of the main control volume of temperature, and the grids were dispersed identically at the two sides of the center line. The positions of the two channel plates were carefully located so that the two plates were strictly symmetric about the centerline. In such cases, if the final steady-state solution is asymmetric, this asymmetry may be considered to be caused by some numerically inherent character, rather than any imperfection in geometrical symmetry.

At each time step, iteration convergency was judged by the relative change in the general variables for two successive computations. This relative change was restricted below 10^{-5}.

For the case of entire domain, we have four average Nusselt numbers, the outside average Nusselt number of the left plate, inner average Nusselt number of the left plate, inner average Nusselt number of the right plate and the outside average Nusselt number of the right plate. They are named as Nu_{OL}, Nu_{IL}, Nu_{IR} and Nu_{OR}, respectively.

The plate average Nusselt numbers were defined as:

$$Nu = \int \left| \frac{\partial \Theta}{\partial X} \right| dY \tag{7}$$

3. Results and discussion

The numerical investigation was performed for the case of $Ra = 2 \times 10^4$, 2×10^5 and 10^6, the solutions were analyzed as follows.

3.1 Ra 2×10^4, steady and symmetrical solution

For the case of Ra< = 2×10^4, the numerical investigation revealed that the unsteady process approached steady symmetrical field. The velocity field and isotherms of such solution were shown in Figure 2 (a and b). Such results are in good agreement with the steady numerical investigation with symmetrical boundary condition (Figure 3, a and b).

3.2 Ra = 2×10^5, a complex periodical asymmetric solution

A simulation of the natural convection from the zero initial fields was performed for Ra = 2×10^5. Although the initial field was symmetric, the natural convection turns to asymmetry after a short time. When time approaches infinite, an asymmetric periodical solution was obtained. The history of the dimensionless temperatures at the three points shown in Figure 1 is shown in Figure 4(a). The flow fields (stream function contour) at different instant of cycle of this solution are shown in Figure 4(b).

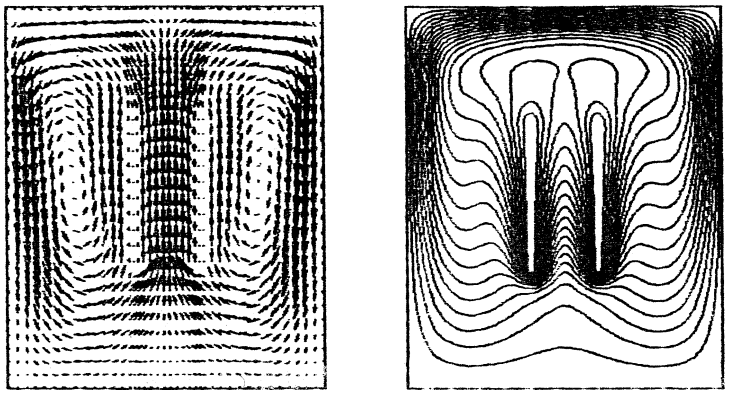

Figure 2.
Predicted flow fields and isotherms with steady governing equations: (a) velocity vectors (Ra = 2×10^4); (b) isotherms

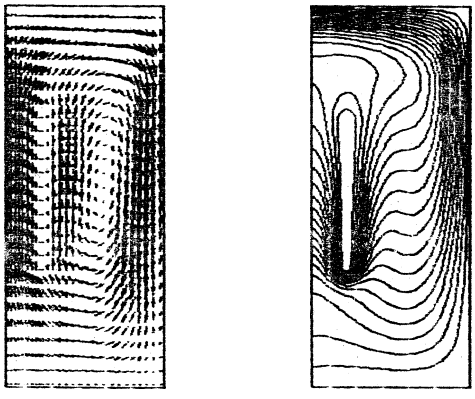

Figure 3.
Predicted steady flow fields and isotherms with transient governing equation (Ra = 2×10^4) (a) velocity vectors; (b) isotherms

3.3 Ra = 10^6, periodical asymmetrical solution

A periodical solution was found for this case when time approached infinite, indicating a Hopf Bifurcation of such configuration. The flow field of the natural convection was also asymmetric.

3.3.1 Periodicity of the solution

The history of the inner average Nusselt number of the right plate in the unsteady natural convection from zero initial field is shown in Figure 5. The data of dimensionless time less than 100 is not shown in this figure for the convenience of presentation. It can be seen from this figure that a periodic solution was approached when time approached infinite. The periodic oscillations of the temperatures of the three points in the middle vertical line (entrance, center and exit of the channel) are shown in Figure 6(a). Figure 6(b) reveals the oscillations of the four average Nusselt numbers. It should be noted that in Figure 6(a), among the three curves of the temperature oscillation, the

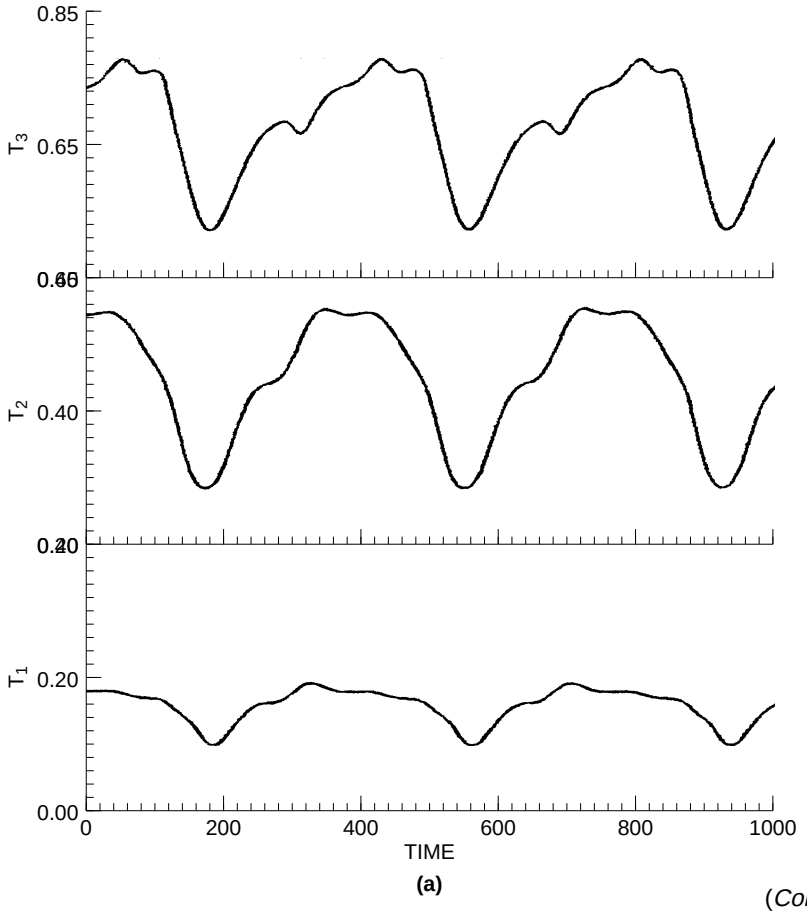

Figure 4.
Solutions for Ra = 2×10^5: (a) oscillating temperatures; (b) oscillating flow fields (stream function)

(*Continued*)

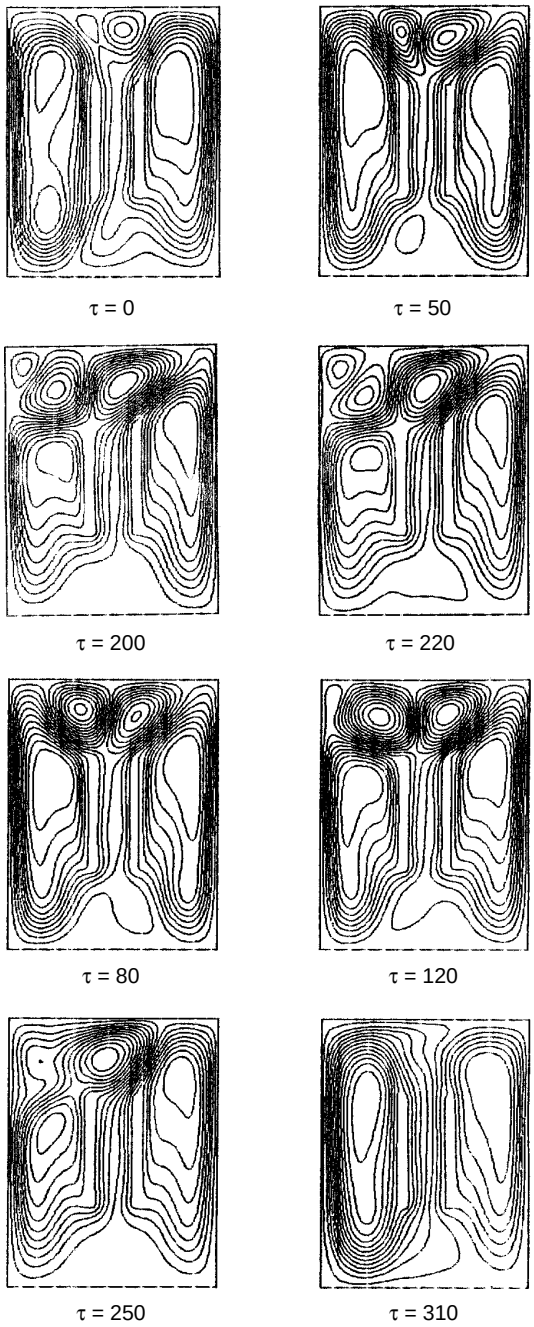

(b)

Figure 4.

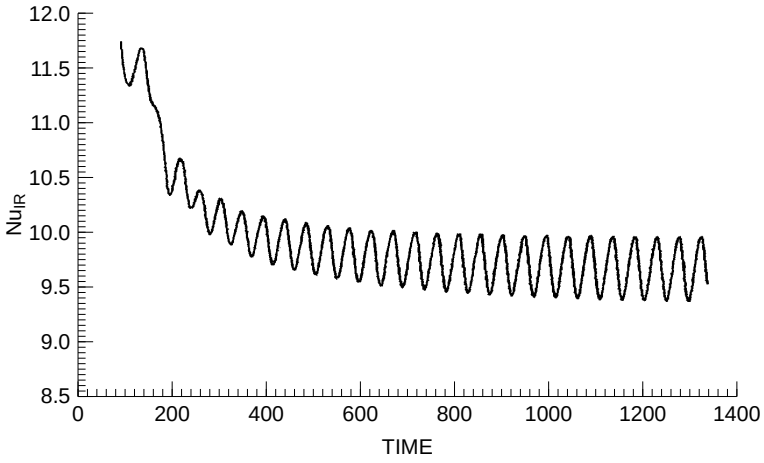

Figure 5.
Evolution history of NU_{IR} for $Ra=10^6$

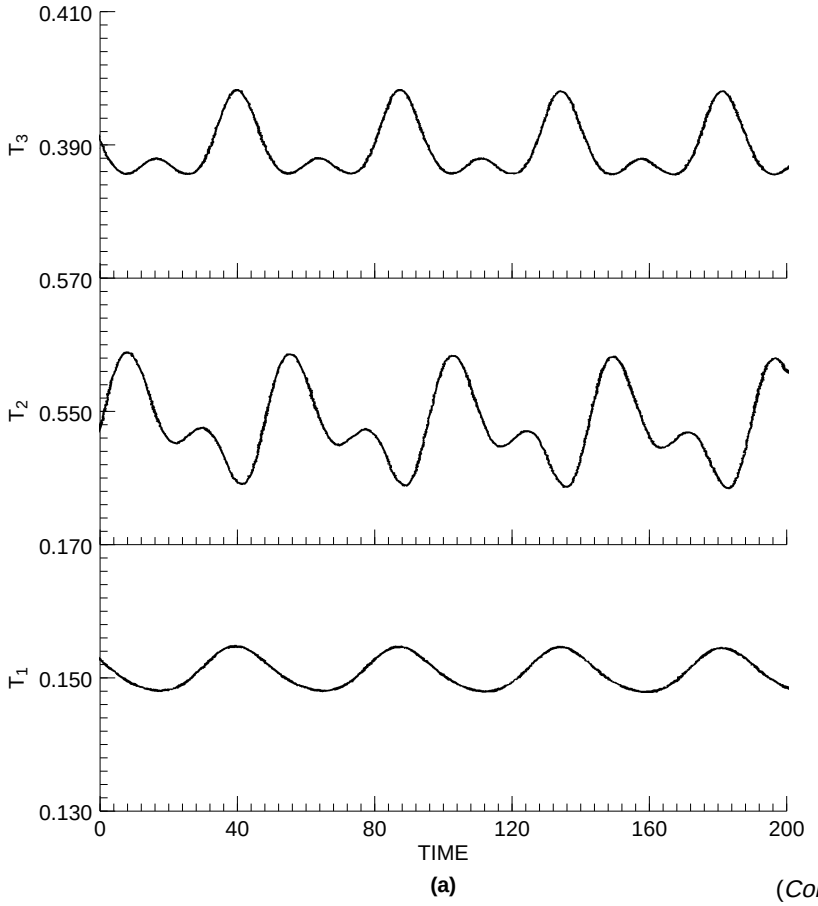

Figure 6.
Predicted temperature and Nusselt number oscillations ($Ra=10^6$): (a) temperature; (b) Nusselt number

(*Continued*)

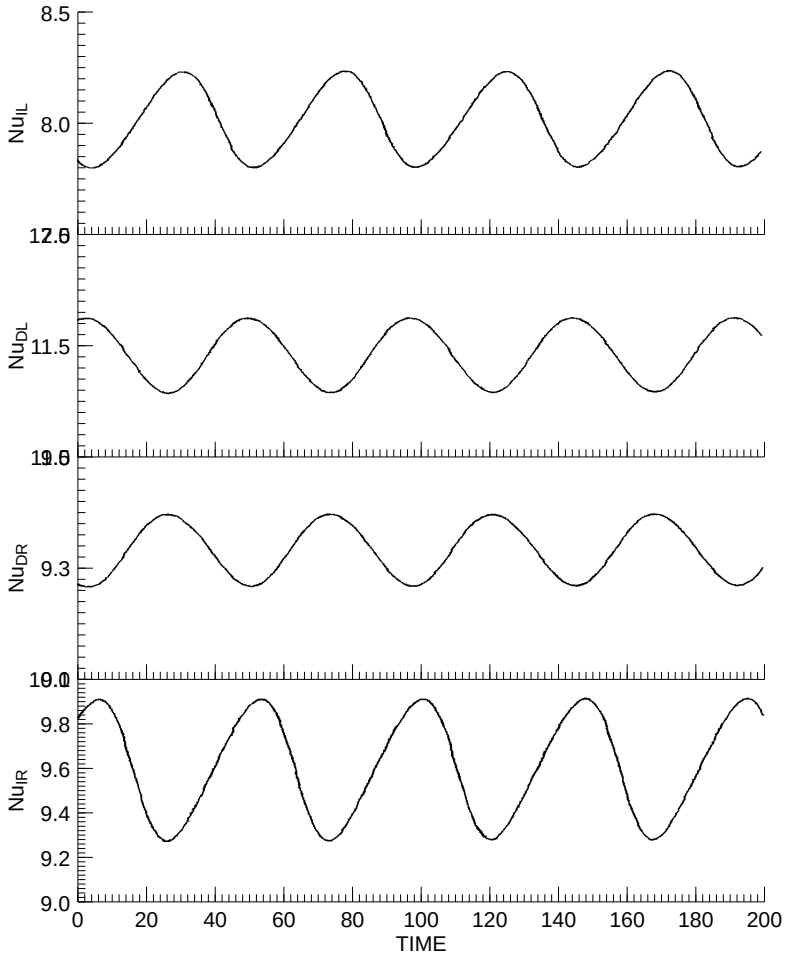

Figure 6.

amplitudes of T_2 and T_3 oscillations are much greater than that of T_1, revealing that the temperature oscillation was weak at the inlet of channel, and it became more and more stronger with the increase in the position. The curve of T_1 is of single periodicity, while T_2 and T_3 are of bi-periodicity type.

Figure 7(a,b and c) are the phase trajectories composed by T_2 to T_1, T_3 to T_1 and T_3 to T_2. All the curves are closed, revealing the periodicity of the solution. Since the computation time of the natural convection investigated is limited and finite, the solution is not perfectly periodic and the trajectory in each figure is actually a group of curves. However, it is believed that such a group of curves approach to a single closed one when the computation time approaches infinite.

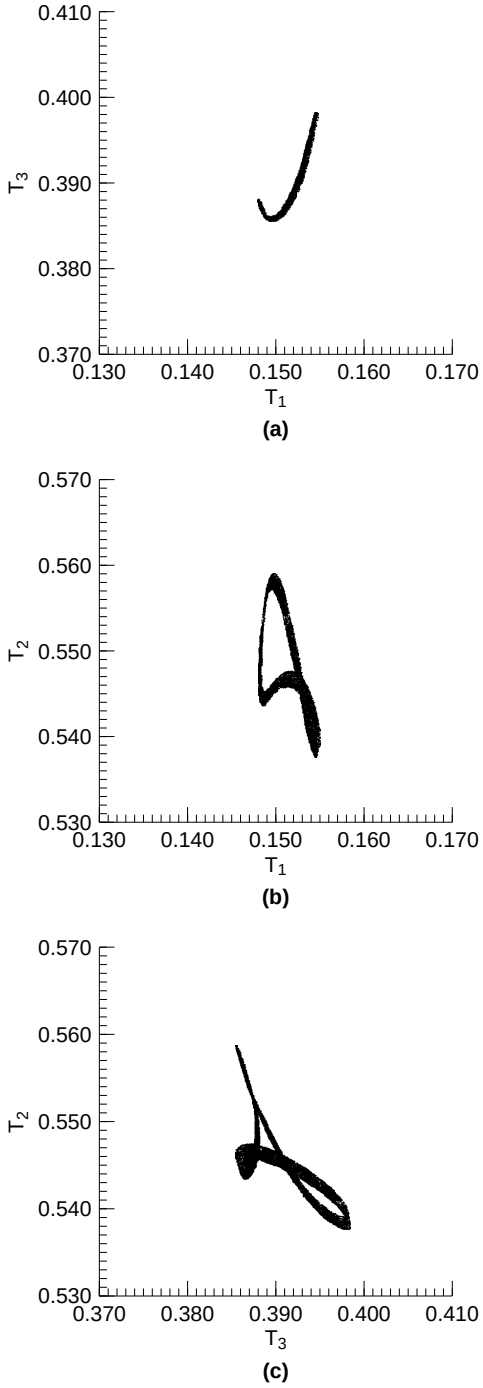

Figure 7.
Oscillation trajectory
(a) T_3 vs. T_1
(b) T_2 vs. T_1
(c) T_2 vs. T_3

The energy spectrum analysis for the oscillations based on fast Fourier transformation (FFT) was conducted to study the periodicity of the unsteady process. Let f(τ) be an oscillation signal, define

$$A_s = \int_0^\infty f(\tau)\sin\frac{2\pi\tau}{\tau_m}d\tau \tag{8}$$

$$A_c = \int_0^\infty f(\tau)\cos\frac{2\pi\tau}{\tau_m}d\tau \tag{9}$$

then

$$A_m = \sqrt{A_s^2 + A_c^2} \tag{10}$$

represents the amplitude of the harmonic component with a period of τ_m. Based on the numerical results for Nu_{IR} with τ greater than 400, a computation was conducted based on the integrations shown in equations (8)-(10). The amplitudes of the harmonic components with series of periods τ_m are shown in Figure 8. According to this figure, two specific periods, 23.5 and 46.7 should be noted, because they represent two local peaks in the energy spectrum. The large value of the periods, 46.7, is the main period, the small value, 23.5, half of the large period, is the harmonic of the oscillation. The short period of the oscillation only appeared in the curves of the history of T_2 and T_3, and cannot be clearly observed in Figure 6(a). It should be pointed out that the curve of the energy spectrum contains somewhat mixed and disordered oscillation compositions, specially for $\tau_m > 70$. This is also caused by the limited computation time. If we

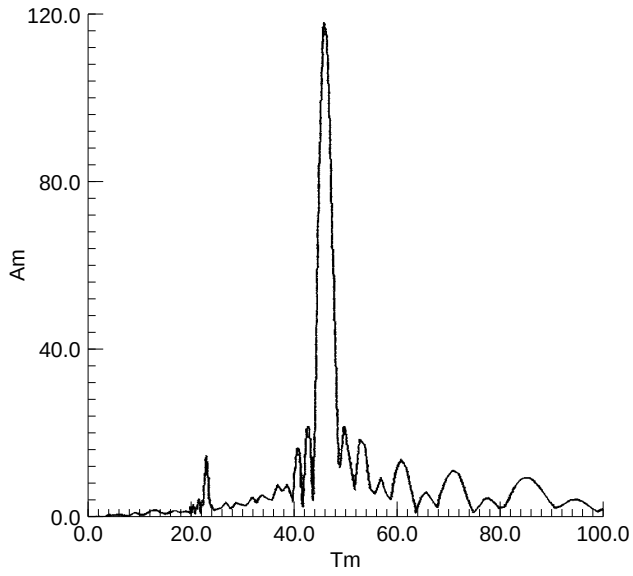

Figure 8.
Energy spectrum for the oscillation at $Ra=10^6$

use a strictly periodic solution and the integration interval of time is long enough, such noise signal will disappear in the energy spectrum.

Attention is now turned to the history of the flow field in a cycle, and Figure 9(a-f) is provided for this purpose. Figure 9 shows the stream function contours at difference steps of a cycle. Basically speaking, there are four big vortices in the enclosure, two outside the channel and two on the top of the channel. Our emphasis will be put on the flow pattern change in the channel. As can be seen

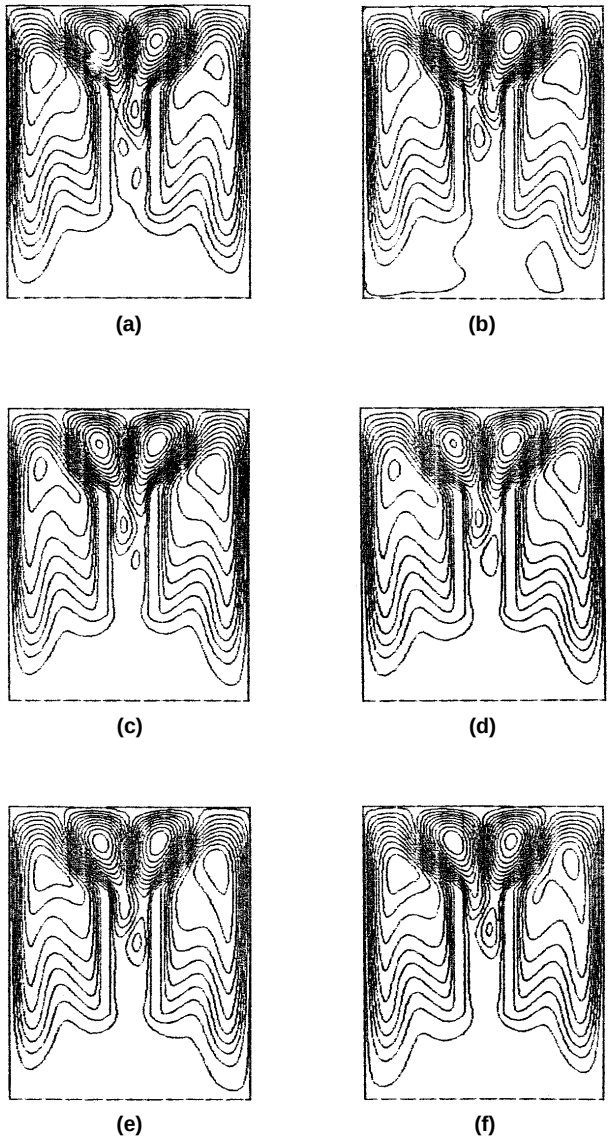

Figure 9.
Evolution of streamfunction in any cycle at $Ra=10^6$: (a) $\tau=0$, at the beginning of a cycle; (b) $\tau=8$; (c) $\tau=16$; (d) $\tau=20$; (e) $\tau=28$; (f) $\tau=30$

from Figure 9(a), under the left top vortex, there is a small vortex near the left plate. The small vortex is then strengthened gradually, moves up along the channel (Figure 9(b)), and merges with the top vortex on the left (Figure 9(c)). Almost at the same time, near the right plate, another small vortex is formed. This small vortex grows up, merges with the top vortex of the same side (Figure 9(d-f)). Such process is repeated again and again, leading to the flow oscillation. The temperature field will also be altered periodically as depicted by Figures 10(a-f). It may be noted that the oscillation of the inner Nusselt numbers of the plates are closely related to these flow pattern oscillations. Since the moving up and merging of the small vortex with the corresponding top one occur alternately at the left and right, the inner Nusselt numbers of the two plates thus have an opposite phase in their oscillation curves (Figure 6(b)).

3.3.2 Asymmetry of the solution

The history of the temperature field in Figure 10(a-f) in one cycle reveals the asymmetry of the solution. In Figure 6(b), the history of Nu_{IR}, Nu_{OR}, Nu_{OL} and Nu_{IL} also reveals such character. If the solutions were symmetrical, the values of the two inner average Nusselt numbers should be equal. Also the average values of the two outside Nusselt numbers should be the same. However, this is not the case. The mean value of Nu_{IR} was 9.6, that of Nu_{IL} was 8.0. The difference between them is about 20 per cent. The difference between the average outside Nusselt numbers of the two plates was also in the order of 20 per cent. If the symmetry boundary condition is used and only half of the enclosure is taken as the computation domain, the solution asymmetry cannot be revealed and our numerical practice also shows that for the case of $Ra = 10^6$ the bifurcation to oscillatory flow will not occur. Therefore, the adoption of symmetry boundary condition should be considered very carefully.

The numerical results obtained by Le Quere and Alziary de Roquefort (1986) show that for natural convection of air in differentially heated rectangular cavities of aspect ratio 1 to 2 and with conducting top and bottom walls, the critical Rayleigh number at which unsteady flow appears is of the order of 2×10^6. Our numerical practices have shown that the existence of the isolated internal channel can promote the occurrence of the unsteady flow at a lower Rayleigh number. This observation is of great practical importance, since configurations like the one studied in this paper are often encountered in engineering. Both numerical study and experimental verification have now been conducted by the present authors for different types of such configurations. Furthermore, the oscillating process for the case of $Ra = 2 \times 10^5$ is more complex than that of $Ra = 10^6$. One possible reason for this unusual phenomenon may be that the bicellular flow pattern is not stable at low Rayleigh numbers. More research work will need to be performed in order to understand it thoroughly and this is also under way in the authors' research group.

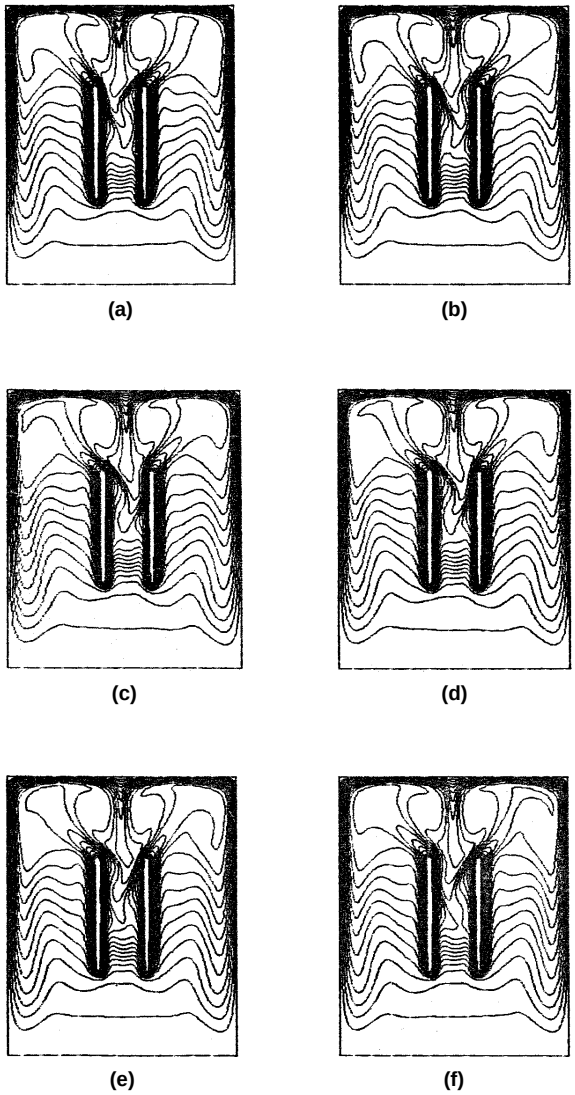

Figure 10.
Evolution of isotherms in any cycle at $Ra=10^6$: (a) $\tau=0$, at the beginning of a cycle; (b) $\tau=8$; (c) $\tau=16$; (d) $\tau=20$; (e) $\tau=28$; (f) $\tau=30$

4. Conclusions

The following conclusions may be obtained:

(1) The natural convection in the configuration studied is steady and symmetric for small Rayleigh numbers (at least Ra up to 10^4), and it turns to asymmetrical periodic flow for enough high Rayleigh numbers (say $Ra = 2 \times 10^5$) and bifurcates to an oscillatory flow.

(2) The existence of the internal isolated channel in the enclosure may promote the occurrence of the unsteady flow of natural convection at a lower Rayleigh number.

(3) The oscillating solution for Ra = 10^6 contains two periods, τ_m = 46.7 and 23.5. The short period was half of the long period.

(4) A cycle of the periodic natural convection at Ra = 10^6 includes the evolution of small vortices in the channel (appearing, moving up and merging with the top vortex). And it is this evolution of small vortices that leads to the oscillation of fluid temperature and Nusselt number.

References

Adlam, J.H. (1986), "Computation of two-dimensional time-dependent natural convection in a cavity where there are internal bodies", *Computers & Fluids,* Vol. 14, pp. 142-57.

Henkes, R.A.W.M. and Hoogendoorn, C.J. (1990), "On the stability of the natural convection flow in a square cavity heated from the side", *Applied Scientific Research,* Vol. 47, pp. 195-220.

Le Quere, P. and Alziary de Roquefort, T. (1985), "Transition to unsteady natural convection of air in differentially heated vertical cavities", *4th Int. Conf. on Numerical Method in Laminar and Turbulent Flow,* Pineridge Press, pp. 841-52.

Le Quere, P. and Alziary de Roquefort, T. (1986), "Transition to unsteady natural convection of air in vertical differentially heated cavities, influences of thermal boundary conditions on the horizontal walls", *8th Int. Conf. Heat Transfer,* San Francisco, CA, pp. 1533-8.

Liu, J.P. and Tao, W.Q. (1996), "Numerical analysis of natural convection around a vertical channel in a rectangular enclosure, heat and mass transfer", (to be published).

Shyy, W. and Rao, M.M. (1993), "Simulation of transient natural convection around an enclosed vertical channel", *ASME J. Heat Transfer,* Vol. 115, pp. 946-54.

Winters, K.H. (1987), "Hopf bifurcation in the double-glazing problems with conducting boundaries", *ASME J. Heat Transfer,* Vol. 109, pp. 894-8.

Yang, K.T. (1988), "Transitions and bifurcations in laminar buoyant flows in confined enclosure", *ASME J. Heat Transfer,* Vol. 110, pp. 1191-1204.

Yang, M. and Tao, W.Q. (1992), "A numerical study of natural convection heat transfer in a cylindrical enclosure with internal concentric slotted hollow cylinder", *Numer. Heat Transfer,* Vol. 22, Part A, pp. 289-306.